ADVANCED FUNCTIONAL MATERIALS
www.afm-journal.de

Self-Healing and Stretchable Molecular Ferroelectrics with High Expandability

*Zhongxuan Wang, Haochen Yang, Long Zhu, Qian Wang, Lina Quan, Po-Yen Chen, and Shenqiang Ren**

The interplay between crystal ordering and stretchability is frequently encountered in contemporary materials science, particularly in the case of ferroelectrics. The inherent dilemma arises when these materials need to withstand repetitive mechanical deformations or stretching without sacrificing their crystal integrity, all while retaining their remarkable ferroelectric properties and even exhibiting self-healing capabilities. This complexity further presents a significant challenge in the design and engineering of mechanically rigid molecular ferroelectric crystals, particularly for applications where both precise crystalline structure and mechanical adaptability are crucial. In this study, the humidity-controlled expansion and contraction, dissolution, and recrystallization of a self-assembled molecular ferroelectric-in-hydrogel framework are reported. Self-healing ferroelectric-in-hydrogel networks exhibit a recyclable humidity-tailored ionic conductivity from 2.86×10^{-6} to 1.36×10^{-5} S cm^{-1}, facilitating the stretchable piezoelectric sensing. Additionally, the dynamic bond reforming interactions are observed, leading to the tailoring of Young's modulus from 452 to 170 MPa, maintaining ferroelectricity under a strain of 20% with a piezoelectric coefficient of 15.7 pC N^{-1}. Upon lattice contraction, the molecular contacts undergo reforming, leading to the restoration of stretchable ferroelectrics/piezoelectrics and paving the way for stretchable bioelectronics for full-body motion monitoring. The capabilities highlighted here open avenues for stretchable and self-healing ferroelectric-in-hydrogel bioelectronic technologies.

1. Introduction

Molecular ferroelectric materials are attracting significant attention for their applications in flexible sensors and wearable electronic devices due to their outstanding attributes such as lightweight, synthetic versatility, and biocompatibility, making them promising candidates for soft robotics and electronic skin applications.[1] However, to date, only ferroelectric polymers intrinsically meet these flexibility requirements.[2] The ferroelectric polarization in molecular ferroelectrics arises from symmetry breaking within the molecular crystal lattice.[3] This polarization, along with the unique ferroelectric properties, originates from the highly ordered crystal structure, which relies on the alignment of molecular dipoles and symmetry breaking within the lattice. However, this highly ordered structure is prone to mechanical failure under stress, rendering the material mechanically brittle and unable to withstand bending, stretching, or other deformations. Consequently, developing flexible molecular ferroelectric crystals has been highly challenging.[4] This challenge stems from the widely accepted principle that enhanced crystal ordering is often achieved at the expense of flexibility, and vice versa. Achieving a balance between high crystal order and mechanical adaptability is thus a central consideration in designing stretchable ferroelectrics. Furthermore, molecular ferroelectric materials require self-healing capabilities to endure repeated cycles of mechanical strain and electric field application. However, most molecular ferroelectric materials lack intrinsic self-healing

Z. Wang, L. Zhu, S. Ren
Department of Materials Science and Engineering
University of Maryland
College Park, MD 20742, USA
E-mail: sren@umd.edu

The ORCID identification number(s) for the author(s) of this article can be found under https://doi.org/10.1002/adfm.202417180

DOI: 10.1002/adfm.202417180

H. Yang, P.-Y. Chen
Department of Chemical and Biomolecular Engineering
University of Maryland
College Park, MD 20740, USA

H. Yang, P.-Y. Chen
Maryland Robotics Center
College Park, MD 20740, USA

Q. Wang, L. Quan
Department of Chemistry
Virginia Tech, Blacksburg
Blacksburg, VA 24060, USA

Q. Wang, L. Quan
Department of Materials and Science Engineering
Virginia Tech, Blacksburg
Blacksburg, VA 24060, USA

properties, making it difficult for them to recover their original properties following bending or deformation. The inherent self-healing and mechanical flexibility of flexible matrices offer a promising approach to overcome these limitations of molecular ferroelectrics, creating a synergistic effect that combines the unique advantages of both materials.[5] The resulting composite material not only demonstrates excellent mechanical resilience but also retains the high performance of the molecular ferroelectric phase. This research thus presents a novel design platform for the flexible applications of molecular ferroelectrics, effectively overcoming the limitations posed by their inherent brittleness.

Notably, hydrogels characterized by a cross-linked 3D polymer network, effectively imparts flexibility by lowering its Young's modulus[6] while exhibiting ionic conductivity.[7] Its distinctive combination of ionic conductivity and mechanical stretchability makes it an ideal choice for crafting bioelectronics.[8] Moreover, the porous network within the hydrogel creates conducive conditions for the aqueous growth of molecular ferroelectric/piezoelectric crystals. Simultaneously, its ion channel serves as a pathway to bridge ionic conductivity and the piezoelectric effect in ferroelectric component. Here, we report self-assembled molecular ferroelectric $ImClO_4$ crystals (IM) into polyvinyl alcohol (PVA) hydrogel to prepare self-healing and stretchable ferroelectric-in-hydrogel networks (IM-in-PVA, stretching up to 50% strain). The ionic conductivity of IM-in-PVA can reach 2.86×10^{-6} S cm^{-1} at room temperature while ferroelectric properties are observed persistently at temperatures below 373 K. The piezoelectric coefficient of IM-in-PVA can reach $^{-}15.7$ pC N^{-1}. Moreover, the Young's modulus, ferroelectric polarization, and ionic conductivity of the IM-in-PVA can be effectively tuned by the relative humidity (RH). The dynamic bonding interaction between IM molecules and hydrogel networks imparts the new capability to undergo expansion, contraction, self-healing, and recrystallization, thereby allowing the customization of ionic conductivity, piezoelectric characteristics, and mechanical properties. With increasing humidity, the ion conductivity can increase from 2.86×10^{-6} to 1.36×10^{-5} S cm^{-1}. Meanwhile, the mechanical properties of IM-in-PVA are also can be tuned by humidity. The Young's modulus decreases from 452 to 170 MPa with increasing humidity. Owing to their simultaneous tunability in ionic conductivity, ferroelectricity, and mechanical flexibility, our stretchable ferroelectrics with the optimum piezoelectric coefficient d_{33} of 15.7 pC N^{-1} provide a valuable strategy for developing wearable bioelectronics. Stretchable IM-in-PVA sensors can effectively monitor the voltage signals generated by full-body movements, enabling effective monitoring of the amplitude and frequency of motion. This capability not only promotes the functional applications of flexible ferroelectric materials but also serves as a catalyst for advancing the field of stretchable and self-healing ferroelectric materials.

2. Results and Discussion

Polyvinyl alcohol-based hydrogels are colloidal dispersions characterized by a 3D network structure formed through the cross-linking and swelling (**Figure 1**a). The cross-linking of PVA can be achieved by modifying hydroxyl groups with a cross-linking agent. The acids containing hydroxyl functional groups serve as chemical crosslinking agents.[9] The reactive carboxyl groups in these acids undergo esterification with the hydroxyl groups of PVA, forming diverse inter-/intramolecular covalent bonds that establish the cross-linking structure between PVA polymer molecules. The cross-linking process is influenced by factors such as the amount of cross-linking agent, time, and reaction temperature.[10] In the depicted process (Figure 1a), IM-in-PVA ferroelectric hydrogels were prepared by dissolving PVA with IM in water and allowing a slow evaporation through the temperature gradient. The abundant water and perchloric acid induced the cross-linking reaction of PVA, leading to the formation of a hydrogel structure with a rich polymeric network. During the water evaporation process, numerous IM molecules enter the PVA network structure and crystallize, thereby contributing to the formation of a dense structure within PVA networks (Figure S1, Supporting Information). The IM-in-PVA network structure formed by the cross-linking of IM and PVA can tailor its mechanical properties, ionic conductivity, and ferroelectricity by humidity, as shown in Figure 1b,c. The volume of the PVA hydrogel expands due to water absorption, leading to the volume expansion of the IM-in-PVA ferroelectric hydrogel networks. Upon absorbing an excessive amount of water molecules, the IM crystals dissolve, giving rise to the formation of an ionic liquid. It is noteworthy that the modulation of mechanical properties, ferroelectricity, and ionic conductivity of IM-in-PVA through humidity is a reversible process. After the water is released through annealing, the IM ionic liquid within the PVA hydrogel network undergoes re-crystallization, leading to the formation of IM molecular ferroelectric crystals. The synergistic interplay between the unique attributes of ionic conductivity and piezoelectricity within the IM-in-PVA creates a dynamic platform for advancing bioelectronic sensing technologies. The inherent ability of the material to conduct ions facilitates the transmission of piezoelectric signals, while its piezoelectric characteristics enable responsiveness to mechanical stimuli. This dual functionality opens avenues for the development of sensitive and responsive bioelectronic sensors. The responsive nature of the material allows for the creation of bioelectronic sensors capable of detecting subtle changes in the surrounding environment or physiological conditions.

Figure 2a,b display cross-sectional and surface scanning electron micrographs (SEM) image of the IM-in-PVA. Closely packed columnar IM crystals (≈5 to 10 μm in size) are observed within the surrounding PVA hydrogel network. Figure S2 (Supporting Information) provides a cross-sectional energy dispersive X-ray spectroscopy mapping (ESD) of IM-in-PVA, confirming the extensive distribution of chlorine and nitrogen elements. This phenomenon likely results from the evaporation process, wherein the solution reaches saturation, triggering the organized growth of IM crystals in columnar structures enveloped by the PVA hydrogel network. Consequently, a dense and uniform IM-in-PVA film is formed (Figure S2, Supporting Information). The XRD patterns of IM-in-PVA, as depicted in Figure S3 (Supporting Information), exhibit diffraction peaks at 16.5°, 19.4°, 22.5°, 24.5°, 28.2°, 32°, 33.8°, and 36.2°, corresponding to the (100), (−110), (110), (111), (111), (200), and (−210) crystal planes of IM crystals, respectively. The peak at 19.4° corresponds to the (101) crystal plane of PVA.[11] The FTIR spectra of IM-in-PVA are presented in Figure 2c. A C—H vibrational peak is observed $^{-}2840$ cm^{-1}. The peak in the vicinity of 1750–1735 cm^{-1} is attributed to the stretching vibrations of the double bond C═O and C—O from

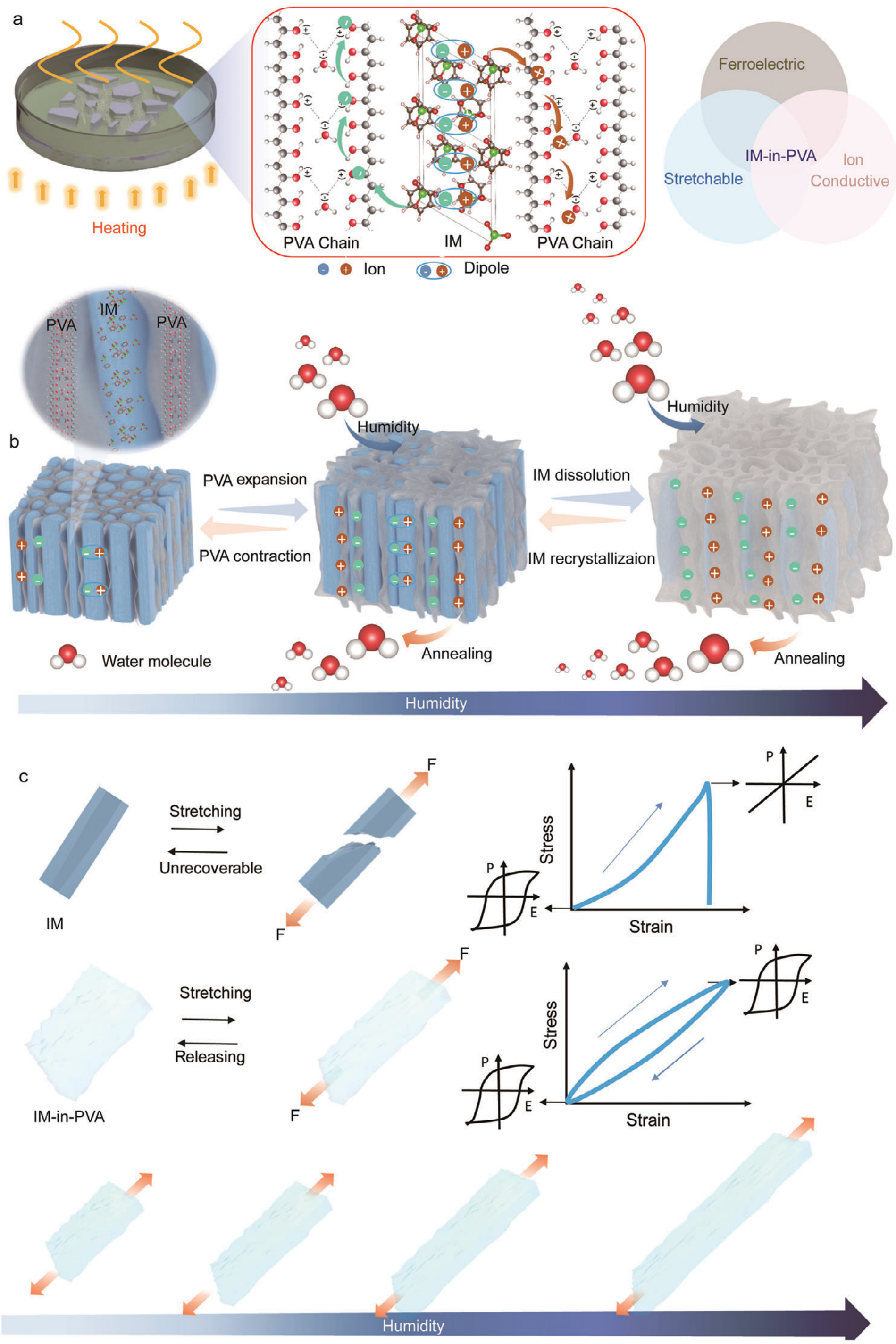

Figure 1. Self-assembly synthesis and humidity-reversible modulation of IM-in-PVA. a) Self-assembly synthesis of flexible IM-in-PVA films. b) Volume and self-healing evolution of IM-in-PVA during the water absorption and release cycles for expansion and contraction, dissolution, and recrystallization process. Inset is the schematic diagram of ionic channel within hydrogel networks. c) Mechanical flexibility of IM-in-PVA. Compared to molecular ferroelectric crystals, IM-in-PVA exhibits excellent mechanical flexibility and elasticity.

the acetate group remaining from PVA (Figure S4, Supporting Information).[12] Due to the abundance of free hydroxyl groups within the PVA, a distinct -OH absorption peak is observed ~3255 nm^{-1} in IM-in-PVA (Figure S4, Supporting Information). This phenomenon arises from hydrogen bonding interactions among hydroxyl groups between PVA chains, confirming the formation of the hydrogel. Furthermore, characteristic absorption peaks of IM crystals are also observed in the FTIR spectra, indicating the coexistence of PVA and IM ferroelectric crystals in IM-in-PVA. Due to the presence of PVA hydrogel, IM-in-PVA exhibits

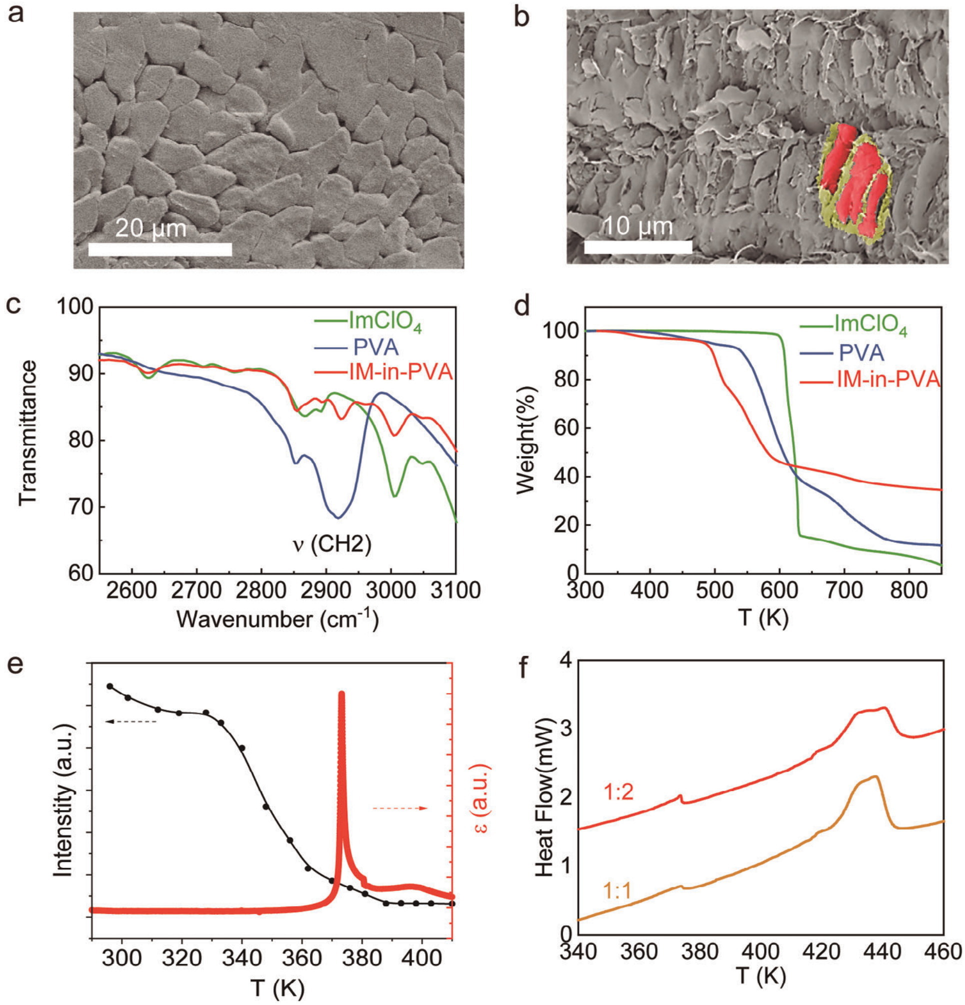

Figure 2. Ferroelectricity, thermal, and optical characterizations of IM-in-PVA. a) SEM image showing the surface morphology of IM-in-PVA, revealing tightly arranged IM crystals (PVA:IM = 1:1 w/w). b) Cross-sectional SEM image of the IM-in-PVA, showing columnar arrangement of IM crystals surrounded within a PVA hydrogel network (PVA:IM = 1:1 w/w). The red region represents IM crystals, while the yellow region represents the PVA hydrogel. c) FTIR spectrum of IM-in-PVA (PVA:IM = 1:1 w/w). d) Thermogravimetric analysis of PVA, IM and IM-in-PVA (PVA:IM = 1:1 w/w). e) Temperature dependent SHG spectra and dielectric constant of IM-in-PVA (PVA:IM = 1:1 w/w). f) The influence of the mass ratio of PVA to IM on the phase transition temperature during the DSC measurements with different mass ratios.

a 3% weight loss at 380 K, attributed to water molecules captured by the hydrophilic hydroxyl groups within the PVA hydrogel. A significant 50% weight loss is observed ~583 K, indicating the decomposition of IM ferroelectric molecules within the IM-in-PVA. Besides its flexibility, IM-in-PVA exhibits ferroelectric properties. Figure S5 (Supporting Information) displays the polarization-electric field (P-E) hysteresis loops of IM-in-PVA at room temperature, confirming its room temperature ferroelectric ordering. Second harmonic generation (SHG), a second-order nonlinear optical effect highly sensitive to structural symmetry, is commonly considered a prerequisite for determining ferroelectric material polarity. As shown in Figure 2e and Figure S6 (Supporting Information), the IM-in-PVA exhibits a pronounced SHG signal, while the SHG signal diminishes above 373 K, indicating a change in the symmetry of IM-in-PVA.[13] This suggests a ferroelectric phase transition temperature of 373 K from the ferroelectric to paraelectric phase when the temperature above 373 K.

A distinct dielectric constant peak of IM-in-PVA is observed at 373 K due to ferroelectric-paraelectric phase transition of IM (Figure 2e). In the differential scanning calorimetry (DSC) curve of IM-in-PVA, the phase transition processes of both IM and PVA are observed (Figure 2f). A distinct exothermic and endothermic peak is evident ~373 K, indicative of the ferroelectric and dielectric phase transitions within the IM ferroelectric crystals. Additionally, an exothermic peak is observed ~426 K, corresponding to the melting process of PVA. As the IM mass ratio increases from 33.3% (PVA:IM = 1:2 m m^{-1}) to 50% (PVA:IM = 1:1 m m^{-1}), the melting peak of PVA shifts to higher temperatures. This may be attributed to the increased IM content, leading to a denser internal structure of the PVA, requiring higher temperatures for melting.[14]

The substantial hydrogel network in IM-in-PVA enables it to capture a significant amount of water molecules, resulting in deformation. **Figures 3a** and S7 (Supporting Information) illustrate

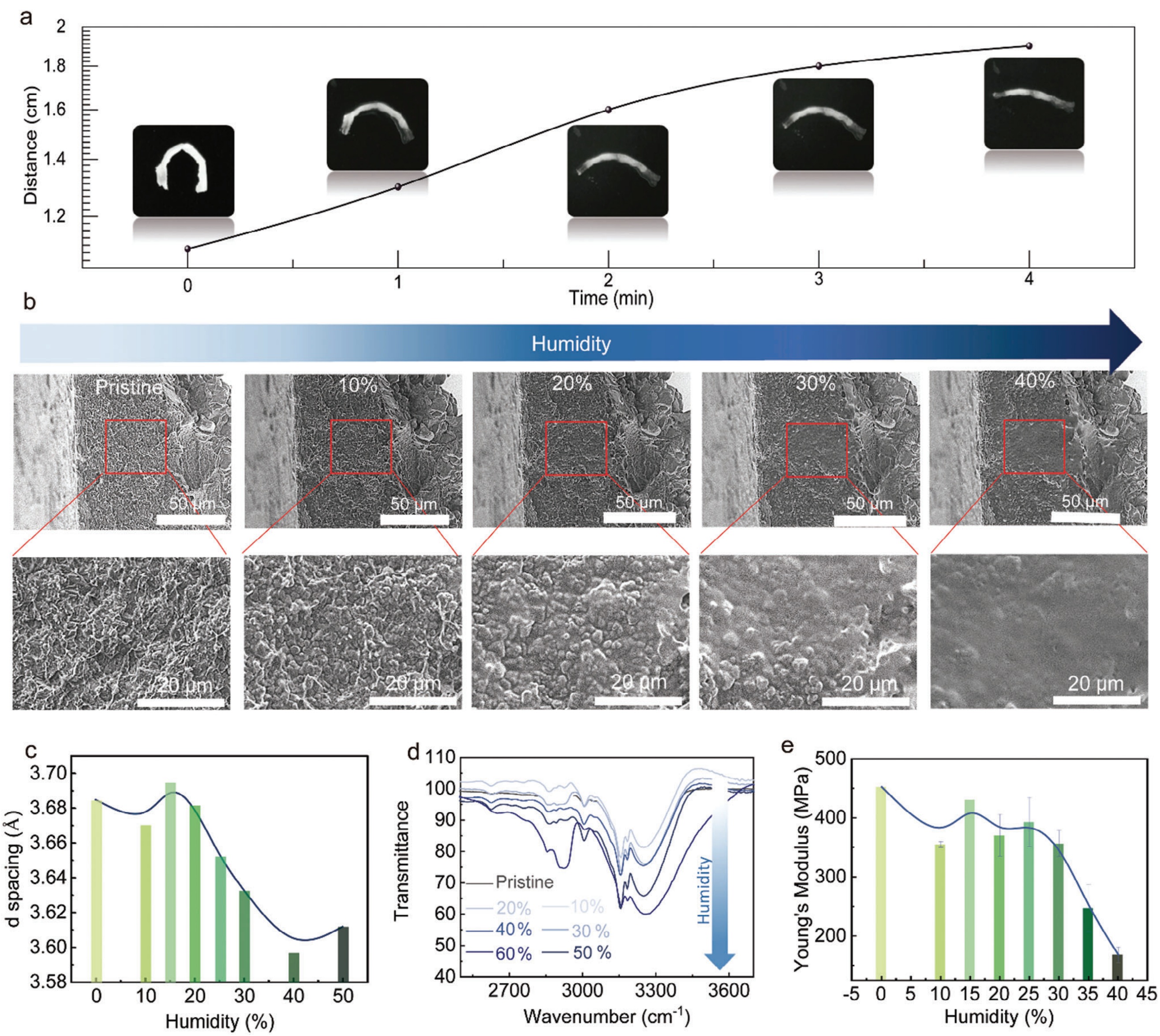

Figure 3. Moisture-induced deformation and structural changes in IM-in-PVA (PVA:IM = 1:1 w/w). a) The deformation of IM-in-PVA fibers after absorbing moisture in a 60% relative humidity environment. The distance between the ends of the IM-in-PVA fiber increases continuously due to the expansion of PVA caused by water absorption. b) The cross-sectional SEM image of IM-in-PVA after moisture absorption. c) The expansion of IM-in-PVA polymer after water absorption results in a reduction in the d spacing (110) of IM crystals. d) Humidity dependent FTIR spectra of IM-in-PVA. e) Humidity modulation Young's Modulus of IM-in-PVA.

that when IM-in-PVA was exposed to an environment with 60% relative humidity, the polymers gradually unfolded over time as they absorbed more water, transitioning from a curved shape. The IM-in-PVA also became transparent due to the absorption of a substantial amount of moisture. To investigate the causes of this absorption-induced deformation, SEM of IM-in-PVA was conducted after exposure to environments with different RH levels for the same duration. Figure 3b depicts SEM images of IM-in-PVA exposed to moisture at different RH levels. Water absorption by the surrounding hydrogel leads to an overall increase in dimensions of the IM crystal surface. The SEM images indicate a substantial increase in grain size as RH rises, attributed to the enveloping effect of PVA hydrogel around IM crystals. The expansion of the IM crystal surface due to water absorption by the surrounding hydrogel leads to an overall increase in dimensions. When the RH reaches 40%, extensive water absorption by PVA forms a PVA hydrogel film covering the entire surface of IM-in-PVA. This phenomenon is attributed to the encapsulation of IM crystals by the PVA hydrogel. Upon absorbing a substantial quantity of water molecules, hydroxyl groups within the PVA hydrogel engage in hydrogen bonding with water molecules. This interaction prompts the reorganization of PVA polymer molecules, enlarging the space between them and, consequently, resulting in volume expansion. The volumetric expansion of the PVA hydrogel upon water absorption results in the deformation and continuous extension of IM-in-PVA. As shown in Figure 3c and Figure S8 (Supporting Information), with RH increasing from 10% to 50%, the diffraction peak corresponding to the (110) plane shifts from 24.2°to 24.8°. The d-spacing corresponding to the (110) plane decreased from 3.68 to 3.61 Å. This suggests a continuous reduction in the lattice constant of IM crystals as PVA hydrogel absorbs water. This may be attributed to the volumetric expansion of the PVA hydrogel surrounding the IM crystals, resulting in compression of the IM crystal lattice.[15] The increased hydroxyl groups within the PVA after water absorption contribute to a notable enhancement in the intensity of the -OH absorption peak observed in FTIR (Figure 3d). The softening effect induced by water absorption in PVA leads to an exponential decrease in the Young's modulus, leading to the IM-in-PVA softer and more stretchable with increasing water content. Figure 3e shows that the Young's modulus of IM-in-PVA decreases from 452 to 170 MPa as RH increases from 10% to 40%. The mechanical rigidity of PVA hydrogel primarily arises from the hydrogen bonding and crystalline regions between its polymer chains. Upon absorption of water molecules, these hydrogen bonds are disrupted and partially degraded, facilitating greater mobility of the polymer chains and consequently decreasing the overall stiffness and Young's modulus. The infiltration of water molecules induces swelling in the hydrogel matrix, increasing the intermolecular distances between chains, thereby weakening intermolecular interactions and further diminishing the Young's modulus of the material.[16] This phenomenon indicates a significant influence of RH on the mechanical properties of IM-in-PVA. This sensitivity to RH can be attributed to the presence of hydrogen bonds in the hydrogel, facilitating ion conduction.

Figure 4a illustrates that as exposure time increases in an 80% high RH environment, IM-in-PVA absorbs more water, causing the dissolution of IM ferroelectric molecular crystals. With continuous absorption of water by the hydrogel, the IM crystals gradually dissolve, therefore, the X-ray diffraction peaks associated with IM ferroelectric molecules disappeared. Subsequently, as water molecules evaporate, the IM molecules within the PVA hydrogel network undergo recrystallization. Consequently, the diffraction peaks corresponding to the IM molecular ferroelectric crystals emerge and progressively intensify with extended annealing time. This suggests the potential for humidity-induced self-healing of IM-in-PVA. Figure 4b depicts the gradual transparency of the IM-in-PVA as they absorb a significant amount of water molecules. With increasing annealing time and extensive water evaporation, the IM-in-PVA transitions from a transparent to an opaque state (Figure S9, Supporting Information). The PVA hydrogel serves as an ion conductor, enhancing the ion channels in the IM-in-PVA ferroelectric crystal and creating favorable conditions for detecting electrical signals from the IM ferroelectric crystal. In humid environments, the IM-in-PVA ferroelectric crystal absorbs water molecules, further enhancing its ionic conductivity. Additionally, when the material undergoes deformation, the piezoelectric effect of the IM component generates piezoelectric signals, transmitted through ions as a conductive medium (Figure 4c). When the IM-in-PVA ferroelectric material absorbs molecules, the ion content increases. Due to the enhanced ion channels generated by the PVA hydrogel, the ionic conductivity rises progressively with increasing humidity (Figure 4d). As the RH increases from 0% to 50%, the ion conductivity increases from 2.86×10^{-6} to 1.36×10^{-5} S cm^{-1} (Figure 4d,e). Due to the water-soluble nature of IM crystals, the water content in the PVA hydrogel also affects the ferroelectric properties of IM crystals. As shown in Figure 4f and Figure S10 (Supporting Information), we present the ferroelectric loops of IM-in-PVA at different RH, revealing the RH-dependent behavior of ferroelectric polarization in IM-in-PVA. The remnant polarization gradually decreases after reaching a maximum of ≈0.9 μC cm^{-2} at 10% RH. This indicates that at lower RH levels, the hydrogel absorbs a certain amount of water molecules, which increases the ion conductivity of the hydrogel and leads to a larger remnant polarization. However, the IM crystals gradually dissolve at high RH level, disrupting the ferroelectric crystal structure and subsequently reducing the remnant polarization. the remnant polarization decreases to $^{-}$0.4 μC cm^{-2} at an RH of 60%. Importantly, the modulation of ferroelectric polarization in IM-in-PVA by humidity is a reversible process. PVA is a transparent film, and IM crystals are transparent crystals (Figure 4g; Figure S11, Supporting Information). When IM is introduced into PVA hydrogel, the IM-in-PVA film turns white (Figure 4g). Molecular ferroelectric crystals lack flexibility, making them unsuitable for flexible devices. However, the integration of molecular ferroelectric crystals with hydrogel offers an effective solution to this challenge, enabling the coexistence of molecular ferroelectricity and stretchability. Due to the ability of IM crystals to form an ordered structure, with each IM crystal enveloped by PVA hydrogel, the mechanical properties of IM-in-PVA are inevitably influenced by the content of IM crystals. The PVA hydrogel network make it have excellent mechanical properties, capable of being stretched by over 400% (Figure 4h). There is a reduction in the tensile strength of IM-in-PVA with increasing IM content. This phenomenon may be attributed to the presence of a substantial amount of IM crystals hindering the formation of a dense hydrogel network, thereby diminishing the tensile properties of IM-in-PVA. As shown in Figure 4i, the IM-in-PVA exhibits ease of bending and can endure various degrees of torsion. The structure of the IM-in-PVA remains stable even after being twisted 180 degrees. This lays the foundation of flexible electronics for molecular ferroelectrics. Figure 4j presents the results of cyclic stretching tests conducted on IM-in-PVA at a 5% elongation. Notably, the loading/unloading curves at 5% strain reveal prominent hysteresis loops, indicating substantial energy dissipation in the IM-in-PVA. The capacity for energy dissipation is a crucial indicator for evaluating the mechanical performance of cross-linked IM-in-PVA. The cyclic stretching tests demonstrate that the cross-linking interactions effectively dissipate energy during the stretching process, further confirming the outstanding mechanical performance of IM-in-PVA. Figure 4k and Figure S12 (Supporting Information) are the P-E loops of IM-in-PVA under different tensile strains. The ferroelectric polarization of IM-in-PVA remains constant at a 30% tensile strain. However, when subjected to a 40% strain, the polarization intensity initiates a decline. Under higher tensile stress, significant internal deformations in IM-in-PVA damages the ion conduction pathways at the IM-in-PVA interface, resulting in decreased polarization intensity. The remarkable combination of mechanical performance, ion conductivity, and ferroelectricity positions IM-in-PVA with promising applications in electronic skin, wearable sensors, and soft robotics. The integration of mechanically brittle molecular ferroelectrics with flexible matrices,

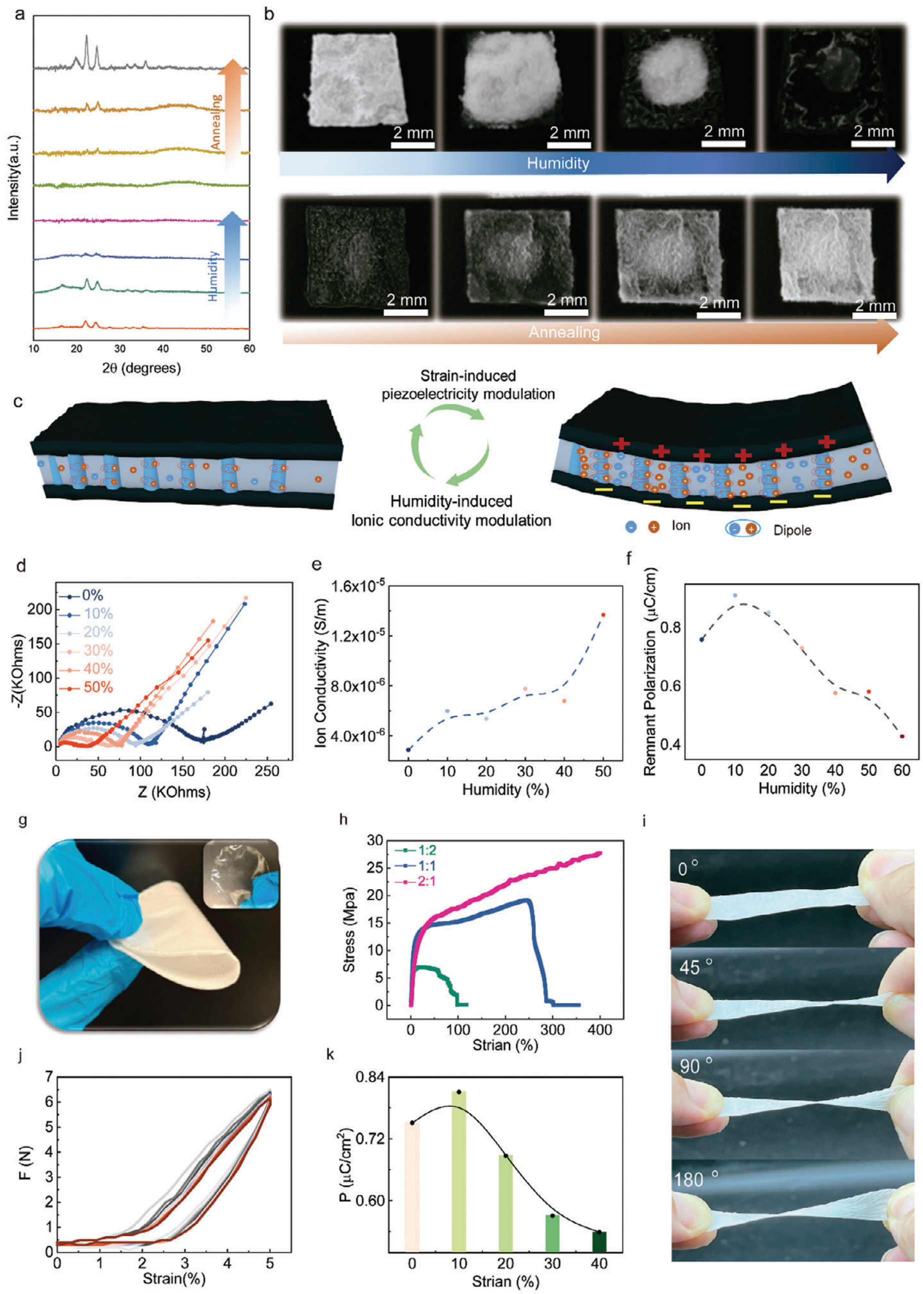

Figure 4. Reversible modulation of structure, ionic conductivity, ferroelectric properties, and mechanical flexibility in IM-in-PVA by moisture content (PVA:IM = 1:1 w/w). a) The dissolution and subsequent recrystallization of IM crystals within the IM-in-PVA due to water absorption and loss processes during XRD measurement. The annealing temperature is 90 °C. b) Photograph of the IM dissolution after water absorption and recrystallization after loss water in IM-in-PVA. The annealing temperature is 90 °C. c) Strain-induced piezoelectricity and humidity-induced ionic conductivity modulation of IM-in-PVA film. d) and e) Humidity modulation of IM-in-PVA ion conductivity. f) Humidity modulation remnant polarization of IM-in-PVA. g) The incorporation of IM crystals has transformed the PVA film from transparent to white. h) Tensile strength of IM-in-PVA with different mass rate of PVA and IM. i) Photograph of PVA-in-IM ferroelectric polymer which remains stable after twisting beyond 180 degrees. j) The cyclic stretching tests of PVA-in-IM ferroelectric polymer. k) Stretching modulation remnant polarization of IM-in-PVA.

such as hydrogels possessing self-healing properties and mechanical flexibility, offers a novel platform for applying molecular ferroelectric materials in flexible devices. This approach could potentially be extended to other molecular ferroelectric and flexible matrix systems. Several essential conditions need to be met in preparing molecular ferroelectric–flexible material composites. First, there should be a strong interaction between the molecular ferroelectric and the flexible matrix, such as hydrogen bonding or electrostatic interactions, to provide a driving force for co-assembly into an ordered structure. This molecular interaction

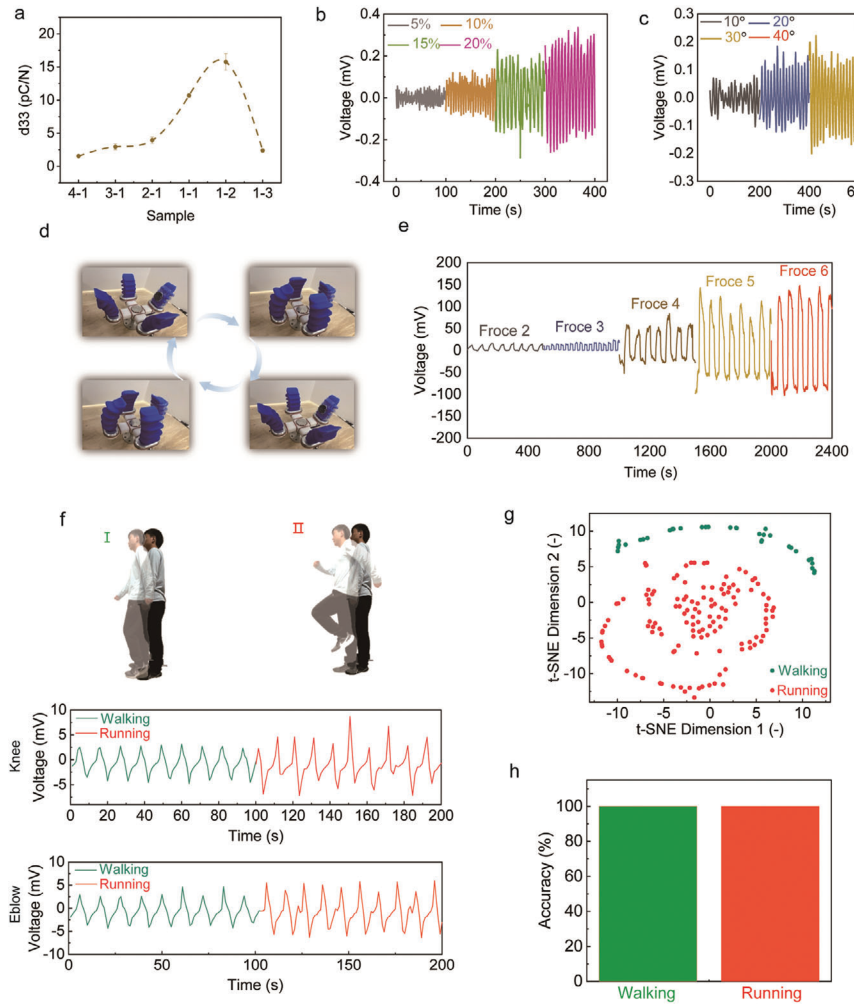

Figure 5. Piezoelectric characteristics and applications of IM-in-PVA polymer in body motion monitoring. a) The d_{33} piezoelectric coefficient of IM-in-PVA polymer with different mass ratios of PVA and IM. b) Change in output voltage caused by the stretching induced strain of IM-in-PVA polymer sensor (5%–20% strain) (PVA:IM = 1:1 w/w). c) The voltage output of IM-in-PVA polymer sensor at different bending angles (10°–40°) (PVA:IM = 1:1 w/w). d) Image of robotic hand movement characterized in Figure (e). e) The voltage output of IM-in-PVA due to the motion of robotic hand. Force level (force 2 to force 6) represents the degree of deformation of the robotic hand (PVA:IM = 1:1 w/w). f) Body motion monitoring based on IM-in-PVA ferroelectric hydrogels. I and II represent the voltage output caused by the movement of the elbows or knees during walking and running, respectively (PVA:IM = 1:1 w/w). g) t-SNE scatterplot of two body motions, where the strain sensing data underwent the dimension reduction into two dimensionless parameters (i.e., t-SNE dimensions 1 and 2). h) The prediction accuracies of ANN for two boy motions.

is crucial for establishing a stable, high-performance composite system. Second, the flexible matrix should exhibit a degree of ionic conductivity, enabling effective transmission and detection of the piezoelectric signals generated by the deformation of the molecular ferroelectric. This ionic conductivity is fundamental to the reliable application of molecular ferroelectric composites in wearable devices, soft robotics, and other flexible electronic devices. By meeting these design conditions, molecular ferroelectric and flexible material composites can achieve efficient mechanical responsiveness and signal output, paving the way for high-sensitivity, reusable flexible sensors and other advanced material applications.

Figure 5a illustrates the d_{33} piezoelectric coefficient at different mass ratios of PVA and IM. As the IM content increases, the piezoelectric coefficient exhibits an initial rise followed by a decrease, reaching an optimal value at a mass ratio of 1:2. This is attributed to the enhancement of ionic channels in the PVA hydrogel network.[17] Figure 5b,c show stress and bending dependent voltage results under varying degrees of tensile and flexural strain. As the tensile strain increases from 5% to 20%, the voltage rises from 0.05 to 0.25 mV. Similarly, when the flexural angle is increased from 10° to 40 degrees, the voltage increases from 0.04 mV to ⁻0.2 mV. Under tensile or flexural deformation, the IM crystals experience varying degrees of compression due to the deformation of the PVA hydrogel network, leading to the generation of piezoelectric effects which can be used in motion sensing and monitoring. As shown in Figure 5d, we affixed a IM-in-PVA film onto the robotic hand. Under different grasping motions of the robotic hand, the IM-in-PVA experiences varying degrees of pressure, thereby generating a voltage output. As shown in Figure 5e and Figure S13 (Supporting Information), the voltage output increases with a higher bending load on the robotic hand, increasing from ≈10 mV to −100 mV. Therefore, the measured voltage output can be used to monitor the grasping motion of the robotic hand. As shown in Figure 5e, we can separately detect the frequency and magnitude of movements at the elbow and knee. During the transitions from action I to action II, the increasing frequency of movement at the elbow and knee leads similarly corresponds to a greater frequency of voltage readings per unit time. Greater movement of the elbow and knee leads to a larger voltage output of IM-in-PVA ferroelectric sensor. This lays the foundation for the application of IM-in-PVA flexible sensor devices. As shown in Figure 5f, the two IM-in-PVA ferroelectric sensors were able to successfully record the strain sensing signals for two body motions, including (i) running and (ii) walking. To visualize and cluster the IM-in-PVA ferroelectric sensors' data from two body motions, the t-distributed Stochastic Neighbor Embedding (t-SNE), a nonlinear multivariate data dimension reduction method was conducted. After low-dimensional mapping, t-SNE dimensions 1 and 2 were plotted in Figure 5g and two distinct clusters corresponding to two body motions were illustrated. Afterward, an artificial neural network (ANN) model was trained with the sensor data for the two body motions classification. The ANN model was able to achieve an accuracy of 100% (Figure 5h) with the testing data which was never used for the model training. The accuracy was calculated by Equation (1),

$$Accuracy = 100\% - \frac{1}{N}\sum_{N}^{i=1}\left|P_i - T_i\right| \tag{1}$$

where $\boldsymbol{P_i}$ is the predicted type of ith body motion by ANN model, and $\boldsymbol{T_i}$ is the recorded label of body motion in testing data (for running $\boldsymbol{P_i},\boldsymbol{T_i} = 0$; for walking $\boldsymbol{P_i},\boldsymbol{T_i} = 1$).

3. Conclusion

In this work, we prepared a self-healing and stretchable ferroelectric-in-hydrogel (IM-in-PVA) by integrating self-assembled molecular ferroelectric IM crystals into PVA hydrogel. The 3D polymer network of PVA facilitates ion conductivity, enabling the transmission of ionic signals of IM ferroelectric crystals. IM-in-PVA polymers exhibit ionic conductivity (2.86×10^{-6} S/cm) and persistent ferroelectric properties below 373 K. It retains its ferroelectric properties even under stretching of up to 20% strain. The piezoelectric coefficient of the IM-in-PVA molecular ferroelectric hydrogel can reach 15.7 pC N^{-1}. Tunability is achieved by adjusting water content, allowing recoverable modulation of mechanical flexibility, ionic conductivity, and piezoelectricity. The ion conductivity of IM-in-PVA rises from 2.86×10^{-6} to 1.36×10^{-5} S cm^{-1} with increasing humidity, while the remnant polarization decreases from 0.9 to 0.4 μC cm^{-2}. The resulting self-healing and stretchable ferroelectrics provide a promising platform for biological sensor devices, with flexible piezoelectric sensors effectively monitoring human body movements.

4. Experimental Section

Synthesis of $ImClO_4$ Crystals: IM crystals were synthesized by dissolving one mole of imidazolium chloride (97%) in deionized water (200 mL), followed by the addition of one mole of perchloric acid to the imidazolium chloride solution. The mixture was stirred for 10 min, after which IM crystals were formed by slowly evaporating the aqueous solution.

Synthesis of IM-in-PVA Ferroelectric Hydrogel Polymer: An aqueous solution of PVA (99 + %) at a concentration of 1 g mL^{-1} was stirred at 90 °C for 6 h. Subsequently, it was mixed with varying volumes of a 1 g mL^{-1} aqueous solution of $ImClO_4$ and stirred at 40 °C for another 6 h. The IM-in-PVA ferroelectric hydrogel was obtained by gradually evaporating the mixture of PVA and $ImClO_4$ aqueous solutions in a Petri dish at 40 °C for 12 h.

P-E Loop and Temperature-Dependent Dielectric Constant Measurements: Polarization-electric field (P-E) hysteresis loops were recorded using a Precision LC Ferroelectric Tester, enhanced with a high voltage interface and a Trek 609B high voltage amplifier (Radiant Technologies Inc., USA). The measurement setup allowed for precise control and analysis of the polarization-electric field behavior in the sample. The P-E hysteresis loops were characterized employing the Radiant LC ferroelectric tester, integrated with a high voltage interface and a Trek 609B high voltage amplifier. Temperature-dependent dielectric constant measurements at 10 kHz were conducted utilizing an Agilent 4294A impedance analyzer coupled with a box furnace. The specimens utilized for the temperature-dependent P-E hysteresis loops and dielectric measurements were equipped with silver epoxy electrodes.

Second Harmonic Generation Measurement: Scattered light from samples was collected using a lens pair and directed into a fiber, which transmitted it to the HRS-300 spectrometer equipped with a PyLoN camera system from Princeton Instruments. The laser source, an Astrella-F-1K femtosecond amplifier by Coherent, generated pulses at 1 kHz frequency, adjusted in intensity with a variable ND filter. Excitation utilized an 850 nm long-pass filter from Edmund and a focusing lens. For polarized second harmonic generation (SHG) measurements, an additional linear polarizer and NIR half-wave plate were positioned before the sample.

TGA and DSC Measurement: Thermal transitions were identified through a Perkin Elmer (Shelton, CT) DSC 7 differential scanning calorimeter, with experiments conducted at a heating rate of 5 °C min^{-1}. The assessment of thermal degradation was performed using a thermogravimetric analyzer (TGA) (SDT Q600, TA Instruments., USA) under a N_2 atmosphere.

Data Availability: The data used for model training are available from Zenodo repository: Data for: Stretchable molecular ferroelectrics with high expandability, accessible via https://doi.org/10.5281/zenodo.10819582. The data that support the plots within this paper and other findings of this study are available from the corresponding authors upon reasonable request.

Code Availability: The Python code within this study is available from GitHub (https://github.com/yhcbloom14/self-healing_stretchable_ferroelectric).

Supporting Information

Supporting Information is available from the Wiley Online Library or from the author.

Acknowledgements

Funding: The U.S. Department of Energy, Office of Basic Energy Sciences, Division of Materials Sciences and Engineering supports S.R. under Award DE-SC0024796.

Conflict of Interest

The authors declare no conflict of interest.

Data Availability Statement

The data that support the findings of this study are available from the corresponding author upon reasonable request.

Keywords

dissolution and recrystallization, molecule ferroelectrics, piezoelectrics, self-healing, stretchability

Received: September 13, 2024
Revised: November 12, 2024
Published online: November 24, 2024

[1] a) Z.-X. Gu, N. Zhang, Y. Zhang, B. Liu, H.-H. Jiang, H.-M. Xu, P. Wang, Q. Jiang, R.-G. Xiong, H.-Y. Zhang, *Nat. Commun.* **2024**, *15*, 4416; b) Y. Ai, W.-Q. Liao, Y.-R. Weng, H.-P. Lv, X.-G. Chen, X.-J. Song, P.-F. Li, R.-G. Xiong, *J. Am. Chem. Soc.* **2023**, *145*, 23292; c) W. Gao, L. Chang, H. Ma, L. You, J. Yin, J. Liu, Z. Liu, J. Wang, G. Yuan, *NPG Asia Mater.* **2015**, *7*, e189; d) H.-Y. Zhang, H.-H. Jiang, Y. Zhang, N. Zhang, R.-G. Xiong, *Angew. Chem., Int. Ed.* **2022**, *61*, 202200135; e) Y.-M. You, W.-Q. Liao, D. Zhao, H.-Y. Ye, Y. Zhang, Q. Zhou, X. Niu, J. Wang, P.-F. Li, D.-W. Fu, Z. Wang, S. Gao, K. Yang, J.-M. Liu, J. Li, Y. Yan, R.-G. Xiong, *Science* **2017**, *357*, 306; f) Y. Ai, Y.-L. Zeng, W.-H. He, X.-Q. Huang, Y.-Y. Tang, *J. Am. Chem. Soc.* **2020**, *142*, 13989; g) Q. Pan, Z.-X. Gu, R.-J. Zhou, Z.-J. Feng, Y.-A. Xiong, T.-T. Sha, Y.-M. You, R.-G. Xiong, *Chem. Soc. Rev.* **2024**, *53*, 5781.
[2] a) A. J. Lovinger, *Science* **1983**, *220*, 1115; b) X. Chen, X. Han, Q.-D. Shen, *Adv. Electron. Mater.* **2017**, *3*, 1600460.
[3] a) W.-Q. Liao, Y.-L. Zeng, Y.-Y. Tang, Y.-Q. Xu, X.-Y. Huang, H. Yu, H.-P. Lv, X.-G. Chen, R.-G. Xiong, *Adv. Mater.* **2023**, *35*, 2305471; b) Y.-Y. Tang, P.-F. Li, W.-Q. Liao, P.-P. Shi, Y.-M. You, R.-G. Xiong, *J. Am. Chem. Soc.* **2018**, *140*, 8051; c) H. Lu, C.-W. Bark, D. Esque De Los Ojos, J. Alcala, C.-B. Eom, G. Catalan, A. J. S. Gruverman, *Science* **2012**, *336*, 59; d) W.-Q. Liao, B.-B. Deng, Z.-X. Wang, T.-T. Cheng, Y.-T. Hu, S.-P. Cheng, R.-G. Xiong, *Adv. Sci.* **2021**, *8*, 2102614; e) A. S. Tayi, A. Kaeser, M. Matsumoto, T. Aida, S. I. Stupp, *Nat. Chem.* **2015**, *7*, 281; f) Y. Hu, Z. Guo, A. Ragonese, T. Zhu, S. Khuje, C. Li, J. C. Grossman, C. Zhou, M. Nouh, S. Ren, *PANS* **2020**, *117*, 27204.
[4] a) M. Owczarek, K. A. Hujsak, D. P. Ferris, A. Prokofjevs, I. Majerz, P. Szklarz, H. Zhang, A. A. Sarjeant, C. L. Stern, R. Jakubas, S. Hong, V. P. Dravid, J. F. Stoddart, *Nat. Commun.* **2016**, *7*, 13108; b) S. Horiuchi, Y. Tokura, *Nat. Mater.* **2008**, *7*, 357; c) S. Horiuchi, F. Ishii, R. Kumai, Y. Okimoto, H. Tachibana, N. Nagaosa, Y. Tokura, *Nat. Mater.* **2005**, *4*, 163; d) E. Collet, M.-H. Lemée-Cailleau, M. Buron-Le Cointe, H. Cailleau, M. Wulff, T. Luty, S.-Y. Koshihara, M. Meyer, L. Toupet, P. Rabiller, S. Techert, *Science* **2003**, *300*, 612; e) Z. Zhang, P.-F. Li, Y.-Y. Tang, A. J. Wilson, K. Willets, M. Wuttig, R.-G. Xiong, S. Ren, *Sci. Adv.* **2017**, *3*, 1701008; f) Y. Huang, J. L. Gottfried, A. Sarkar, G. Zhang, H. Lin, S. Ren, *Nat. Commun.* **2023**, *14*, 5041.
[5] a) W. Li, C. Li, G. Zhang, L. Li, K. Huang, X. Gong, C. Zhang, A. Zheng, Y. Tang, Z. Wang, Q. Tong, W. Dong, S. Jiang, S. Zhang, Q. Wang, *Adv. Mater.* **2021**, *33*, 2104107; b) S. Deswal, G. Khandelwal, R. J. I. S. L. Dahiya, *IEEE Sensors Lett.* **2023**, *7*, 1.
[6] a) H. Dechiraju, M. Jia, L. Luo, M. Rolandi, *Adv. Sustainable. Syst.* **2022**, *6*, 2100173; b) W. Kong, C. Wang, C. Jia, Y. Kuang, G. Pastel, C. Chen, G. Chen, S. He, H. Huang, J. Zhang, S. Wang, L. Hu, *Adv. Mater.* **2018**, *30*, 1801934; c) D. J. S. Seliktar, *Science* **2012**, *336*, 1124.
[7] a) C. Yang, Z. Suo, *Nat. Rev. Mater.* **2018**, *3*, 125; b) K. Y. Lee, D. J. J. C. r. Mooney, *Chem. Rev.* **2001**, *101*, 1869; c) X. Yao, S. Zhang, L. Qian, N. Wei, V. Nica, S. Coseri, F. J. A. F. M. Han, *Adv. Funct. Mater.* **2022**, *32*, 2204565.
[8] a) J. J. Paik, B. Jang, S. Nam, L. J. Guo, *Adv. Healthcare. Mater.* **2023**, *12*, 2300076; b) Y. Zhou, C. Wan, Y. Yang, H. Yang, S. Wang, Z. Dai, K. Ji, H. Jiang, X. Chen, Y. J. A. F. M. Long, *Adv. Funct. Mater.* **2019**, *29*, 1806220; c) G. Li, C. Li, G. Li, D. Yu, Z. Song, H. Wang, X. Liu, H. Liu, W. J. S. Liu, *Small* **2022**, *18*, 2101518.
[9] a) N. Wang, Y. Si, J. Yu, H. Fong, B. J. M. Ding, *Mater. Des.* **2017**, *120*, 135; b) S. Xu, L. Shen, C. Li, Y. J. J. o. A. P. S. Wang, *J. Appl. Polym. Sci.* **2018**, *135*, 46159.
[10] S. Suganthi, S. Mohanapriya, V. Raj, S. Kanaga, R. Dhandapani, S. Vignesh, J. J. C. Kalyana Sundar, *ChemistrySelect* **2018**, *3*, 11167.
[11] a) Y. Chen, J. Li, J. Lu, M. Ding, Y. J. P. T. Chen, *Polym. Test.* **2022**, *108*, 107516; b) A. M. Peres, R. R. Pires, R. L. Oréfice, *Carbohyd. Polym.* **2016**, *136*, 210.
[12] H. S. Mansur, C. M. Sadahira, A. N. Souza, A. A. P. Mansur, *Mater. Sci. Eng. C* **2008**, *28*, 539.
[13] a) G.-W. Du, X.-X. Cao, Y.-A. Xiong, J. Yao, Z.-J. Feng, R.-J. Zhou, T.-T. Sha, H.-R. Ji, X. Zhang, Z.-Y. Jing, Q. Pan, *Adv. Mater.* **2024**, *36*, 2401392; b) W. Li, G. Tang, G. Zhang, H. M. Jafri, J. Zhou, D. Liu, Y. Liu, J. Wang, K. Jin, Y. Hu, H. Gu, Z. Wang, J. Hong, H. Huang, L.-Q. Chen, S. Jiang, Q. Wang, *Sci. Adv.* **2021**, *7*, eabe3068.
[14] a) R. K. Tubbs, *J. Polym. Sci. A Gen. Pap.* **1965**, *3*, 4181; b) D. Thomas, E. Zhuravlev, A. Wurm, C. Schick, P. J. P. Cebe, *Polymer* **2018**, *137*, 145.
[15] a) S. Dolabella, A. Borzì, A. Dommann, A. J. S. M. Neels, *Small Methods* **2022**, *6*, 2100932; b) Z. Zhang, B. Peng, X. Ji, K. Pei, P. K. L. Chan, *Adv. Funct. Mater.* **2017**, *27*, 1703443.
[16] N. Jain, V. K. Singh, S. Chauhan, *J. Mech. Behav. Mater.* **2017**, *26*, 213.
[17] a) B. Bao, J. Hao, X. Bian, X. Zhu, K. Xiao, J. Liao, J. Zhou, Y. Zhou, L. Jiang, *Adv. Mater.* **2017**, *29*, 1702926; b) W. Chen, Q. Wang, J. Chen, Q. Zhang, X. Zhao, Y. Qian, C. Zhu, L. Yang, Y. Zhao, X.-Y. Kong, B. Lu, L. Jiang, L. Wen, *Nano Lett.* **2020**, *20*, 5705.